HHS Public Access

Author manuscript

Ultrasound Med Biol. Author manuscript; available in PMC 2018 February 01.

Published in final edited form as:

Ultrasound Med Biol. 2017 February ; 43(2): 469–475. doi:10.1016/j.ultrasmedbio.2016.09.019.

The effects of oxygen on ultrasound-induced blood-brain barrier disruption in mice

Nathan McDannold[*], **Yongzhi Zhang**, and **Natalia Vykhodtseva**

Department of Radiology, Brigham and Women's Hospital, Harvard Medical School, 75 Francis Street, Boston, MA 02115

Abstract

Numerous researchers are investigating the use of microbubble-enhanced ultrasound to disrupt the blood-brain barrier (BBB) disruption and deliver drugs to the brain. This study investigated the impact of using oxygen as a carrier gas for anesthesia on microbubble activity and BBB disruption. Targets in mice were sonicated in combination with administration of Optison microbubbles (100 μl/kg) under isoflurane anesthesia with either oxygen or medical air. A 690 kHz focused ultrasound transducer applied 10 ms bursts at peak pressure amplitudes of 0.46-0.54 MPa (N=2) or 0.34-0.36 MPa (N=5). After sonication of two locations in one hemisphere, the carrier gas for the anesthesia was changed, and the sonications were repeated in the contralateral hemisphere. The BBB disruption, measured via contrast-enhanced MRI, was significantly greater ($P<0.001$) with medical air than with oxygen. Harmonic emissions were also greater with air ($P<0.001$), while the decay rate of the harmonic emissions was 1.5 times faster with oxygen. A good correlation (R^2: 0.46) was observed between the harmonic emissions strength and MRI signal enhancement. At 0.46-0.54 MPa, both the occurrence and strength of wideband emissions was greater with medical air. However, at lower peak pressure amplitudes of 0.34-0.36 MPa, the strength and probability for wideband emissions were higher with oxygen. Little or no effects were observed in histology at 0.34-0.36 MPa. These findings show that use of oxygen as a carrier gas can result in a substantial diminution of BBB disruption. These results should be taken into account when comparing studies from different researchers and in translating this method to humans.

Keywords

Ultrasound; brain; blood-brain barrier; drug delivery; oxygen; anesthesia

Introduction

The combination of ultrasound and intravenously-administered microbubble ultrasound contrast agents to disrupt the blood-brain barrier (BBB) is being investigated by numerous

[*]Corresponding author: Nathan McDannold, 75 Francis Street, Boston, MA 02115, 617-278-0605, njm@bwh.harvard.edu.

groups as a means to enable and target the delivery of drugs to the central nervous system (Hynynen et al. 2001; Burgess et al. 2015). As the BBB is a significant impediment to the use of most drugs in the brain (Abbott and Romero 1996; Pardridge 2010), this method holds great promise for the treatment of brain tumors and other CNS disorders.

Previously, our laboratory reported that the amount of a tracer extravasated into the brain after BBB disruption was significantly higher in animals anesthetized with intraperitoneal injections of ketamine and xylazine compared to animals anesthetized with isoflurane and oxygen (McDannold et al. 2011). We posited that different vascular effects induced by these two protocols may have had an impact on the interactions between the ultrasound field, the microbubbles, and the brain microvasculature. Around the same time, two studies were published showing that the circulation time for ultrasound contrast agents was substantially reduced when subjects were breathing oxygen compared to medical air (Mullin et al. 2011; Itani and Mattrey 2011), which could also explain our results.

The purpose of this study was to test whether the use of oxygen as the carrier gas for isoflurane anesthesia was the reason for the reduced disruption was observed in our earlier study. In experiments in mice, locations were sonicated in one hemisphere and then repeated in the contralateral hemisphere after switching between oxygen and medical air. We also recorded the acoustic emissions to determine whether they paralleled any differences resulting from the breathing of these different gases and to see if the amount of a tracer delivered to the brain was reflected by the strength of harmonic emissions, as has been observed previously (Arvanitis et al. 2012; Sun et al. 2015). Finally, we investigated whether wideband emissions were correlated with vessel damage, as described before (McDannold et al. 2006). These emissions occur during inertial cavitation, the violent collapse of microbubbles that can induce damage (Lele 1987).

Methods

Animals

All experiments were performed in accordance with procedures approved by the Harvard Medical School Institutional Animal Care and Use Committee. The animals were housed, fed, and watered according to the Office of Laboratory Animal Welfare and the Association for Assessment and Accreditation of Laboratory Care regulations. The experiments were performed using male CD-1 mice (36-47g). The animals were initially anesthetized with an i.p. injection of ketamine (100 mg/kg) and xylazine (10 mg/kg). The fur on the head was removed using clippers and depilatory cream, and a catheter was placed in the tail vein. The animal's head was fixed in a Magnetic Resonance Imaging (MRI) compatible stereotactic frame (constructed in-house), and then the mouse was placed on the focused ultrasound (FUS) device. Isoflurane was applied through a nosecone with either oxygen or medical air as the carrier gas. The isoflurane concentration was titrated based on the respiration rate, and was typically 1-2%.

At 1-2 h after the sonications, the animals were deeply anesthetized, euthanized, and the brains were fixed via transcardial perfusion (0.9% NaCl, 250 mL; 10% buffered formalin phosphate, 500 mL) and prepared for paraffin sectioning. Two 5 μm horizontal sections in

the center of each brain were stained with Hematoxylin and Eosin (H&E) and examined for tissue damage.

MRI-guided FUS

FUS exposures (10 ms bursts applied at 1 Hz for 120 s) were started immediately after the administration of the microbubble ultrasound contrast agent Optison (GE Healthcare, Little Chalfont, Buckinghamshire, United Kingdom; dose: 200 μl/kg; diluted 10× in PBS) to disrupt the BBB under MRI guidance. The transcranial sonications were applied using a 690 kHz FUS transducer driven with a function generator (33220A, Agilent, Santa Clara, CA, USA) and amplifier (240L, E&I, Rochester, NY, USA). Electrical power output was measured using a power meter (E4419B, Agilent, Santa Clara, CA, USA) and dual-directional coupler (C5948-10, Werlatone, Patterson, NY, USA). The transducer was mounted on a plastic plate which was attached to a manually-operated, three-axis MRI-compatible positioning system. The mouse in the stereotactic frame was placed supine with the head within a 5×6 cm transmit/receive surface coil, and the system was placed in an animal 7T (Biospec, Bruker, Billerica, MA, USA) MRI. Acoustic coupling was achieved by submersing the transducer and top of the mouse's head in degassed and deionized water. The acoustic power output for the spherically-curved transducer (diameter/radius of curvature: 4/3 cm) was measured using a radiation force balance. Scans of the acoustic intensity were obtained with a 0.2 mm diameter needle hydrophone (HNC-0200, Onda, Sunnyvale, CA, USA). These calibrations were used to estimate the peak negative pressure amplitude at the focus in water (Hynynen 1990). The width and length of the 50% isopressure contours were 2.3 and 10.3 mm. The transducers, MRI coil, and positioning system were assembled in-house.

Peak negative pressure amplitudes of 0.51-0.54 MPa were used in the first animal. This value was selected based on pilot studies with isoflurane and oxygen (data not shown). These exposures resulted in wideband emissions when medical air was used, so the pressure was reduced to 0.46-0.48 MPa in the second animal, and to 0.34-0.36 MPa in the next five. We used two different exposure levels in each hemisphere. However, no meaningful differences in the BBB disruption or acoustic emissions were observed between these two levels, and in the analysis we divided the sonications into two groups: the 8 locations sonicated at 0.46-0.54 MPa in the first two animals, and the 20 locations sonicated at 0.34-0.36 MPa in the next five animals.

Before each experiment, we localized the focal point in the MRI coordinate space by visualizing heating in a silicone acoustic standoff pad using temperature-sensitive MRI. The mouse was then placed on the system and standard anatomical MRI was used to choose the targets. Two sonications were targeted in each hemisphere, one centered in the putamen and one in the thalamus. After the second sonication, we switched from medical air to oxygen (three animals) or vice-versa (four animals). We waited for two minutes or longer between sonications to allow the bubbles to mostly clear from circulation. After the completion of the four sonications, axial T1-weighted RARE images (parameters: Repetition time: 600 ms; echo time: 18 ms; echo train length: 4; field of view: 4 cm; matrix: 128×128; slice thickness: 1 mm; averages: 4) were acquired before and after intravenous injection of Gadopentetic

acid (Gd-DTPA; Magnevist, Bayer Schering Pharma, Leverkusen, North Rhine-Westphalia, Germany; dose: 0.25 ml/kg), an MRI contrast agent that normally does not cross the BBB.

Acoustic emissions recording

A planar (7×7 mm), air-backed passive cavitation detector with a center frequency of 1.48 MHz (bandwidth ±30 kHz) was used to record the acoustic emissions during sonication. The detector was mounted to the side of the transducer, 3.5 cm away from the focal point. The signals were filtered using a passive notch filter (center frequency: 650 kHz, Allen Avionics, Mineola, NY, USA), amplified 25 times (SR445A, Stanford Research Systems, Sunnyvale, CA, USA), and recorded with a high-speed digitizer (PCI-5124, National Instruments, Austin, TX, USA). The time signal, frequency spectrum, and the tracked harmonic and wideband signals were displayed in real-time using software developed in house in Matlab (MathWorks, Natick, MA, USA). The software acquired a set of data without microbubbles and then waited for the user to inject the microbubbles. Once the microbubble injection starts, the strength of the second and third harmonics relative to this baseline data were calculated as described below.

The voltage/time signals were recorded at a sample rate of 5 MHz and converted online to a power spectra ($PSD(f)$) using Fast Fourier Transform and a Hanning window. The relative signal strength (S_n) in dB at the second (n=2) or third harmonic (n=3) for one burst was defined as follows:

$$S_n = \frac{10}{\Delta f} \cdot log_{10}\left(\int_{\Delta f} \frac{PSD(f)}{PSD_{BL}(f)} df\right)$$

where $PSD_{BL}(f)$ is the mean power spectra obtained without microbubbles, and Δf is a frequency band (width: ±150 Hz) around the second or third harmonic. This formalism follows approaches described earlier (Arvanitis et al. 2012; Samuel et al. 2006). For each sonication, a “harmonics score” (H_{sum}), defined as the sum over all 120 bursts of the maximum of S_2 and S_3, was calculated. Wideband emissions were quantified by calculating the average signal in the sensitive band of the detector (1.48 MHz ± 20 kHz). They were expressed as dB and normalized by the average signal in this frequency range of five recordings obtained without ultrasound.

Data analysis

All data analysis was performed in Matlab (MathWorks, Natick, MA, USA). The signal change in MRI after Gd-DTPA administration was measured in a 3×3 voxel region of interest centered on the enhancing spot. For this measurement, the mean enhancement (± standard deviation) relative to a pre-contrast image was determined. Signal change from a non-sonicated region of interest was subtracted from the measurement to remove contributions from Gd-DTPA in the blood stream. MRI signal enhancement and the strength of the harmonic emissions were compared between pairs of sonications with medical air and oxygen using a paired student’s t-test. The MRI signal enhancement and harmonic strength measured at each time point after Gd-DTPA and microbubble administration, respectively,

were compared for the five animals sonicated at 0.34-0.36 MPa using an unpaired student's t-test. The decay rate of the harmonics signals during sonication was found using linear least-squares regression. Based on the findings by Arvanitis et al. (Arvanitis et al. 2012), the MRI signal enhancement after Gd-DTPA injection (SE) and the harmonics score were fit to the equation $SE = a \cdot e^{b \cdot H_{sum}}$, where a and b are constants. This fit, along with 95% confidence intervals, was done using nonlinear least-squares regression.

Results

BBB disruption and harmonic emissions

Example acoustic spectra obtained during sonication and maps of the MRI signal enhancement obtained immediately after the last sonication are shown for two animals in Figure 1. After Gd-DTPA administration, the MRI signal enhancement was substantially greater when the mouse was breathing medical air, and clear BBB disruption was observed in all but one of these sonications. The targets sonicated in the contralateral hemisphere with oxygen, only 7/14 targets were clearly evident, and the amount of contrast enhancement was obviously less. The magnitude of the harmonic emissions was also greater when medical air was used. In the first two animals, where a higher pressure amplitude (0.46-0.54 MPa) was used, strong wideband emissions were observed during some bursts. In the next five animals, the pressure amplitude was reduced to 0.34-0.36 MPa.

Comparison of the MRI signal enhancement after Gd-DTPA administration and the strength of the harmonic emissions for the pairs of sonications is shown in Figure 2. In every case, the MRI signal enhancement was greater when medical air was used. In all but one location, the harmonics were also larger with medical air. The mean MRI and harmonics signals were both significantly larger with medical air than with oxygen ($P<0.001$). No obvious difference was observed for sonications centered in the putamen versus those in the thalamus.

Figure 3A-B show the harmonic signal strength and the MRI signal enhancement, respectively, as a function of time for all of the locations sonicated at 0.34-0.36 MPa (mean ± SD shown). During sonication, the harmonics signal increased rapidly starting a few seconds after microbubble administration before monotonically decaying. The decay rate with oxygen (−0.162 ± 0.004 dB/s), was 1.5 times higher than that measured with medical air (−0.105 ± 0.003 dB/s). The time at which the signal strength was reduced by half was 113 s with medical air vs. 64 s with oxygen. The signal strength was significantly higher ($P<0.05$) shortly after microbubble administration and again during the second half of the sonication (asterisks in Figure 3A). For both experimental groups, the MRI signal enhancement increased over time after Gd-DTPA administration and then plateaued. The signal was significantly higher ($P<0.01$) at each time point for the animals breathing medical air. Figure 3C plots the MRI signal enhancement as a function of the integrated harmonic emissions score (H_{sum}) for all sonications. A good correlation (R^2: 0.46) was observed to an exponential fit; however there was considerable variability.

Wideband emission and histology

Figure 4 plots the strength and the probability for wideband emission. High wideband signals were recorded in the two animals sonicated at 0.46-0.54 MPa, and the signals recorded with medical air as the carrier gas were significantly higher than with oxygen. In contrast, for the five animals sonicated at 0.34-0.36 MPa, both the probability and the strength of wideband emissions were higher during sonications where oxygen was used. At both pressure amplitude ranges, the probability for wideband emissions peaked 10-15s after microbubble administration. However, at the higher pressure range, strong emissions were sometimes observed at later times during sonication.

Histological examination found normal appearing brain tissue in the targets sonicated at 0.34-0.36 MPa except for a few tiny petechiae surrounding some of the capillary blood vessels (Figure 5). Petechiae were found in one of the ten locations sonicated at these pressure amplitudes with oxygen, and in two of the ten locations with medical air. At 0.46-0.54 MPa, all four targets sonicated with medical air had petechiae, and they were more extensive in both number and size than those observed at the lower exposure levels. With oxygen, a single blood vessel with a tiny adjacent erythrocyte extravasation was found in one of the four targets sonicated at 0.46-0.54 MPa. The four locations sonicated at these levels with medical air had high wideband emissions that accompanied the petechiae. However, while high wideband emissions were observed in a location sonicated with oxygen at 0.48 MPa, no petechiae were found there.

Discussion

Previously, we found that sonication of rats anesthetized with ketamine and xylazine resulted in greater BBB disruption, and in some cases, more petechiae than in animals that were anesthetized with isoflurane and oxygen (McDannold et al. 2011). Others have found that microbubble circulation times were reduced in animals breathing oxygen compared to medical air (Mullin et al. 2011; Itani and Mattrey 2011). The results of the present study demonstrate that oxygen can have a profound diminutive effect on BBB disruption and suggests that our earlier study was not due to anesthesia, but instead to the use of oxygen. These results are important when comparing studies from different research teams that use different anesthesia protocols or carrier gases. They should also be taken into account in clinical trials.

The reason that breathing pure oxygen increases the clearance rate of microbubbles is that it results in an increased ventilation/perfusion imbalance and an increased difference between the sum of partial pressures in the blood in comparison to the ambient pressure (Mullin et al. 2011). This imbalance results in a greater driving force for microbubble dissolution. The loss of perfluorocarbon gas in the alveoli may also play a role (Itani and Mattrey 2011). The increased clearance rate was evident in the recordings of the harmonics. The decay rate of the harmonic signals was approximately 1.5 times higher with oxygen than with medical air, and the half-life was reduced by 43%.

The exponential relationship found here between the MRI signal enhancement after Gd-DTPA administration and the harmonics was similar to that observed previously in

macaques (Arvanitis et al. 2012). Others have shown a linear correlation between stable cavitation activity recorded during sonication and subsequent BBB permeability in mice (Sun et al. 2015). While a good correlation was observed here, there was more variability than in the earlier studies. The variability may have been due to the large focal zone in comparison to the size of the mouse head, and signals arising from areas outside the brain may have confounded our readings. In contrast, in the earlier work in macaques the focal zone was completely contained within the brain (Arvanitis et al. 2012), and the earlier mice work used a higher ultrasound frequency (Sun et al. 2015). The signal-to-noise ratio (SNR) of the small detector here may have also been lower than with the larger detector used in the macaque study. Methods to improve the SNR of the detector would be beneficial.

Improving SNR would likely also improve safety monitoring. There were two locations where wideband emissions were not observed, but a small number of tiny petechiae were observed in histology. Assuming the petechiae are produced by inertial cavitation, this finding suggests that our detector was insufficiently sensitive to detect a small number of inertially-cavitating microbubbles. Other cases had wideband emissions above the noise floor, but no petechiae were found in histology. Since we only examined two sections per brain and the focal region was so large and included areas outside the brain, we cannot conclude that there was no inertial cavitation in those cases.

It is interesting that the strength of and the probability for wideband emissions that were detected at 0.34-0.36 MPa were larger when the animals were breathing oxygen, and that in the case shown in Figure 5 petechiae were observed in absence of MRI-detectable BBB disruption. It is not clear why this would be the case. In addition to increasing the clearance rate, changing the carrier gas may alter the microbubbles and their behavior in an ultrasound field. For example, ultrasound microbubbles swell initially when administered intravenously, and the degree of swelling is expected to be less with oxygen as a carrier gas (Mullin et al. 2011). It is also possible that changing the carrier gas changed the properties of the vasculature or altered the cerebral blood flow. It is known that breathing 100% oxygen results in vasoconstriction and reduced cerebral blood flow (Bergofsky and Bertun 1966). We do not know if such effects played any role in our results, and future work is needed to confirm and understand this finding.

This study had limitations. With the low frequency ultrasound transducer used here, strong reflections and standing waves undoubtedly occurred, resulting in uncertainty of the pressure amplitude in the brain (O'Reilly et al. 2010). This uncertainty likely resulted in the variability in BBB disruption observed between animals. Due to time constraints, we were not able to wait for extended periods between sonications or when switching carrier gases, which may have resulted in additional variability in our results. Also, we did not monitor physiological parameters during the sonications, which may have helped to elucidate the causes for the differences observed between these two carrier gases. Some vascular damage may have been missed since we only examined two sections from each brain. However, the large and obvious differences in the findings with medical air and oxygen suggest that these limitations were relatively minor and are unlikely to change our conclusion that the carrier gas used with isoflurane anesthesia can have a profound impact on ultrasound-induced BBB disruption.

Conclusions

The large differences in BBB disruption found here with different carrier gases suggest that the use of oxygen will significantly impede drug delivery after BBB disruption induced by ultrasound and microbubbles. The finding of reduced BBB disruption with oxygen was likely due to an increased microbubble clearance rate, which was 1.5-fold higher than with medical air. The impact of oxygen was also evident during sonication at high pressure amplitudes, where wideband emissions and vascular damage were reduced in comparison with medical air. Interestingly, however, the probability for wideband emissions *increased* with oxygen during sonications at the lower pressure amplitudes that did not result in significant vascular damage. Overall, the correlation between wideband emissions and vascular damage was inconsistent, suggesting perhaps that our passive cavitation detector was not optimal. However, a good correlation (R^2: 0.46) was found between harmonic emissions and MRI signal enhancement after Gd-DTPA administration and may be useful for controlling the procedure. These effects of oxygen are important in considering the findings from different research groups and should be taken into account in moving to clinical trials.

Acknowledgements

This work was supported by NIH grant P01CA174645. The authors thank Chanikarn Power for her assistance with the animals.

Reference List

Abbott NJ, Romero IA. Transporting therapeutics across the blood-brain barrier. Mol Med Today. 1996; 2:106–113. [PubMed: 8796867]

Arvanitis CD, Livingstone MS, Vykhodtseva N, McDannold N. Controlled ultrasound-induced blood-brain barrier disruption using passive acoustic emissions monitoring. PLoS One. 2012; 7:e45783. [PubMed: 23029240]

Bergofsky EH, Bertun P. Response of regional circulations to hyperoxia. J Appl Physiol. 1966; 21:567–572. [PubMed: 5934464]

Burgess A, Shah K, Hough O, Hynynen K. Focused ultrasound-mediated drug delivery through the blood-brain barrier. Expert Rev Neurother. 2015; 15:477–491. [PubMed: 25936845]

Hynynen, K. Biophysics and technology of ultrasound hyperthermia. In: Gautherie, M., editor. Methods of External Hyperthermic Heating. Springer-Verlag; New York: 1990.

Hynynen K, McDannold N, Vykhodtseva N, Jolesz FA. Noninvasive MR imaging-guided focal opening of the blood-brain barrier in rabbits. Radiology. 2001; 220:640–646. [PubMed: 11526261]

Itani M, Mattrey RF. The Effect of Inhaled Gases on Ultrasound Contrast Agent Longevity In Vivo. Mol Imaging Biol. 2011

Lele, PP. Effects of ultrasound on "solid" mammalian tissues and tumors in vivo. In: Repacholi, MH.; Grondolfo, M.; Rindi, A., editors. Ultrasound: Medical Applications, Biological Effects and Hazard Potential. Plenum Pub. Corp.; New York: 1987.

McDannold N, Vykhodtseva N, Hynynen K. Targeted disruption of the blood-brain barrier with focused ultrasound: association with cavitation activity. Phys Med Biol. 2006; 51:793–807. [PubMed: 16467579]

McDannold N, Zhang Y, Vykhodtseva N. Blood-brain barrier disruption and vascular damage induced by ultrasound bursts combined with microbubbles can be influenced by choice of anesthesia protocol. Ultrasound Med Biol. 2011; 37:1259–1270. [PubMed: 21645965]

Mullin L, Gessner R, Kwan J, Kaya M, Borden MA, Dayton PA. Effect of anesthesia carrier gas on in vivo circulation times of ultrasound microbubble contrast agents in rats. Contrast Media Mol Imaging. 2011

O'Reilly MA, Huang Y, Hynynen K. The impact of standing wave effects on transcranial focused ultrasound disruption of the blood-brain barrier in a rat model. Phys Med Biol. 2010; 55:5251–5267. [PubMed: 20720286]

Pardridge WM. Biopharmaceutical drug targeting to the brain. J Drug Target. 2010; 18:157–167. [PubMed: 20064077]

Samuel S, Miller DL, Fowlkes JB. The relationship of acoustic emission and pulse-repetition frequency in the detection of gas body stability and cell death. Ultrasound Med Biol. 2006; 32:439–447. [PubMed: 16530103]

Sun T, Samiotaki G, Wang S, Acosta C, Chen CC, Konofagou EE. Acoustic cavitation-based monitoring of the reversibility and permeability of ultrasound-induced blood-brain barrier opening. Phys Med Biol. 2015; 60:9079–9094. [PubMed: 26562661]

Tung YS, Vlachos F, Choi JJ, Deffieux T, Selert K, Konofagou EE. In vivo transcranial cavitation threshold detection during ultrasound-induced blood-brain barrier opening in mice. Phys Med Biol. 2010; 55:6141–6155. [PubMed: 20876972]

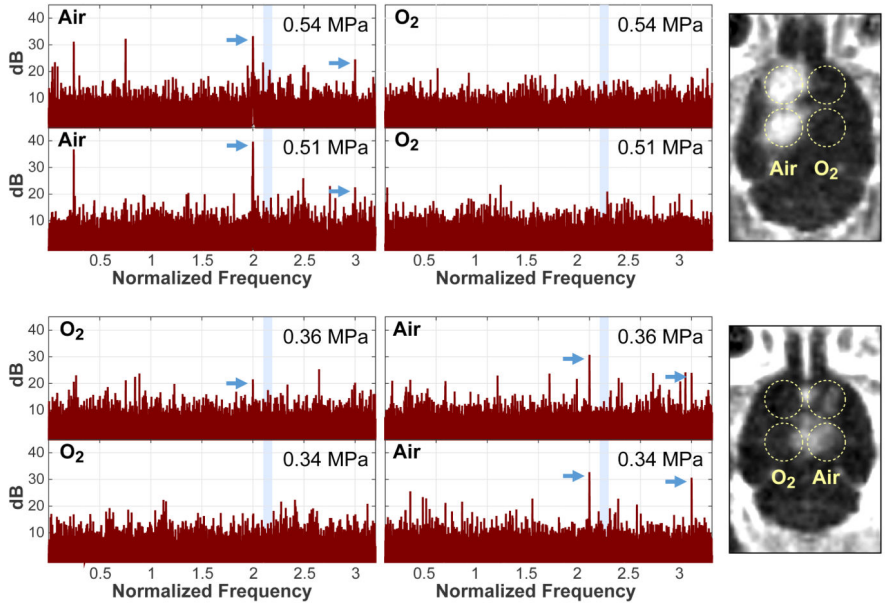

Figure 1.

Example acoustic emission spectra (left) and maps showing MRI contrast enhancement (right) obtained in two mice. In both examples, only the sonications where medical air was used as the carrier gas produced strong harmonics in the emission spectra (arrows) and detectable contrast extravasation in MRI. With oxygen, no or smaller harmonics were observed. The average of all spectra obtained during sonication are shown. They were normalized to spectra obtained without microbubbles. The shaded area in the spectra indicates the resonant frequency of the passive cavitation detector. Activity detected in this band was assumed to be wideband emission.

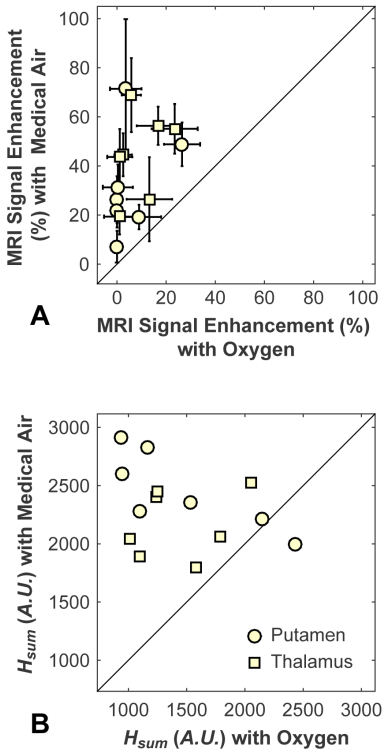

Figure 2.

Comparison of MRI signal enhancement after Gd-DTPA administration (A) and integrated harmonic emissions scores, H_{sum}, (B) between pairs of sonications. In each mouse, two targets were sonicated in each hemisphere. During sonications in one hemisphere, oxygen was used as the carrier gas; in the other hemisphere, it was medical air. In every case, greater MRI signal enhancement was observed with medical air than in the contralateral hemisphere for sonications with oxygen. In all but one case, greater harmonics were observed with medical air. The solid line in each plot indicates unity.

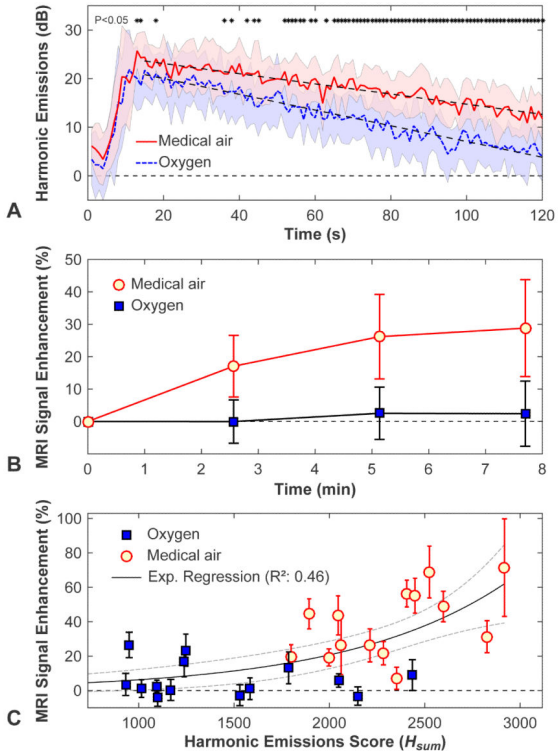

Figure 3.

Comparison of harmonic emissions strength and MRI contrast enhancement in animals breathing oxygen and medical air. (A) Plot showing the average harmonic emission strength (relative to recordings obtained without microbubbles) as a function of time after microbubble injection for all 0.34-0.36 MPa sonications. Shaded areas show the standard deviation, and the dotted lines are linear regressions of the signal decay. Times when the signals recorded in animals breathing medical air were significantly higher ($P<0.05$) are indicated by asterisks. (B) Average MRI signal enhancement plotted as a function of time after Gd-DTPA contrast administration for sonications at 0.34-0.36 MPa (mean ± SD shown). The enhancement was significantly ($P<0.001$) larger for isoflurane and medical air at each time point. (C) For each sonication, the relative harmonic signal vs. time curves were integrated to give a single score. A good correlation (R^2: 0.46) was observed in an exponential fit of the MRI signal enhancement as a function of this score, but substantial variability was observed.

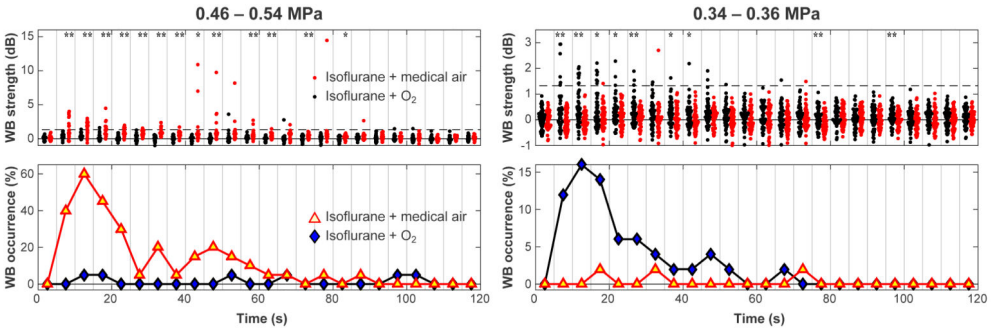

Figure 4.

Comparison of wideband (WB) emissions as a function of time during sonications in mice breathing either oxygen or medical air. Every five recordings were binned, and the probability for wideband emission was found for each bin. The mean signal and number of sonications that had signals greater than two standard deviations above zero were calculated for each bin. This threshold is noted by the dashed line. At the higher exposure levels (N=2 animals, 8 locations), both the strength of the wideband signal and the probability of enhanced emissions were greater in mice breathing air. However, for the locations sonicated at lower pressure amplitudes (N=5 animals, 20 locations), the largest signals were recorded when the mice were breathing oxygen. For each bin, when the signals were significantly different, it is noted by asterisks (* $P<0.05$; ** $P<0.01$).

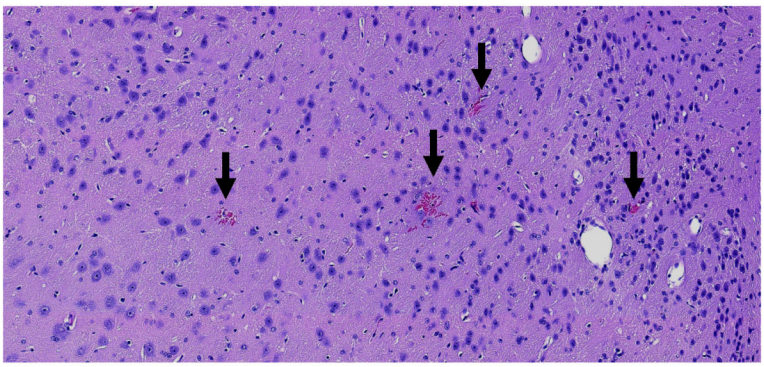

Figure 5.

Microphotograph of an H&E stained section showing petechiae after sonication at 0.36 MPa. These four petechiae, indicated by the arrows, were the only abnormalities detected in the entire section. Such petechiae were found in three of twenty locations sonicated at this exposure range. No other effects were observed. This mouse was breathing oxygen during sonication at this target, and no signal enhancement was detected in MRI after Gd-DTPA administration. No significant harmonic or wideband emissions were recorded. Bar: 100 μm.